**SOLIDS
AND LIQUIDS**

Theoretical Study of Oxygen Sorption and Diffusion in the Volume and on the Surface of a γ-TiAl Alloy

A. V. Bakulin[a,b]*, S. E. Kulkova[a,b], Q. M. Hu[c], and R. Yang[c]

[a] *Institute of Strength Physics and Materials Science, Siberian Branch, Russian Academy of Sciences, Tomsk, 634021 Russia*
*e-mail: bakulin@ispms.tsc.ru
[b] *National Research Tomsk State University, Tomsk, 634050 Russia*
[c] *National Laboratory for Materials Science, Institute of Metal Research, Chinese Academy of Sciences, Shenyang, 110016 China*
Received June 18, 2014

Abstract—The oxygen sorption on the low-index (001), (100), and (110) surfaces of a γ-TiAl alloy is studied by the pseudopotential method with the generalized gradient approximation for the exchange-correlation functional. The most preferred sites for oxygen sorption in the bulk and on the surface of the alloy are determined. The titanium-rich octahedral site is shown to be preferred for oxygen sorption in the bulk material. The effect of the oxygen concentration on the atomic and electronic structures of the stoichiometric TiAl(100) surface is studied. It is shown that, at the first stage of oxidation, oxygen prefers to form bonds with titanium. The energy barriers for oxygen diffusion on the stoichiometric (100) surface and in the bulk of the material are calculated. The energy barriers are shown to depend substantially on the local environments of oxygen and to increase during diffusion from titanium-rich sites. The most possible mechanism of oxygen diffusion from the (100) surface to the bulk of the material is oxygen migration through tetrahedral sites.

1. INTRODUCTION

Ti–Al-based alloys are known to be applied in the aerospace, automotive, and shipbuilding industries and other fields. In addition, titanium aluminides are considered to be promising for hydrogen energetics due to the presence of titanium, which is a hydride-forming element, whereas aluminum has no hydrogen affinity [1, 2]. γ-TiAl-based alloys are most promising, since they have a set of good mechanical properties, including a high strength, plasticity, and heat resistance; a high melting temperature; and a low density [3–5]. Nevertheless, the main disadvantage of these alloys is a low corrosion resistance at high temperatures, which restricts their wider practical application [6, 7]. The available experimental data [6–9] demonstrate that this disadvantage can be caused by the growth of mixed titanium and aluminum oxide layers, since both elements can easily oxidize. Such mixed layers do not ensure a high corrosion resistance at high temperatures, in contrast to α-Al_2O_3. New high-temperature materials are known to be designed using alloying with, e.g., niobium, which has a higher valence as compared to titanium, and using the modification of surface layers [10–13]. Since the growth of oxide films depends on the surface layer composition and defects, surface segregation can substantially affect both the composition and the oxidation of surface layers.

To understand the formation of oxide layers on the γ-Ti surface on a microscopic level, it is necessary to study oxygen adsorption and a possible mechanism of oxygen diffusion into subsurface layers. The adsorption of oxygen is known to be studied on various metallic surfaces, including the Al(111) surface, using ab initio methods [14–18]. The interaction of oxygen with alloy surfaces has received little attention, which is caused by a long computational time [19–24]. The initial stage of oxide layer formation on the γ-TiAl(111) surface was studied in [25, 26], and this stage has received little attention for other low-index surfaces. It is necessary to understand the microscopic nature of the mechanism of oxide growth on the low-index surfaces of a γ-TiAl in order to improve its corrosion resistance. Therefore, to study the interaction of oxygen on an alloy surface depending on its orientation and the surface layer composition and to investigate the diffusion of oxygen into the bulk of the material is a challenging problem.

The purpose of this work is to perform investigation of the oxygen adsorption on the (001), (100), and (110) surfaces in γ-TiAl alloy and to study the effect of the oxygen concentration on the oxidation of the stoichiometric (100) surface and the diffusion of oxygen into the alloy bulk.

2. COMPUTATIONAL DETAILS

The atomic and electronic structures of the low-index surfaces in a γ-TiAl alloy were calculated by the pseudopotential (PP) method using the VASP program code [27–29] with the generalized gradient

Table 1. Calculated elastic constants C_{ij} and bulk modulus B for γ-TiAl

Elastic moduli, GPa	C_{11}	C_{33}	C_{12}	$C_{13}(C_{23})$	C_{44}	C_{66}	B
Our results (PP GGA)	167.2	161.9	81.1	86.3	109.7	65.2	111.5
Theory (FLAPW LDA [45])	190	185	105	90	120	50	126.1
Experiment [46]	187	182	74.8	74.8	109	81.2	111.6
Experiment [47]	187	183	75	75.2	109	81.2	111.9

approximation for an exchange-correlation functional (GGA91) [30]. The cutoff of the kinetic energy was 400 eV. Integration over the Brillouin zone was performed using the Monkhorst–Pack grid [31]. In the case of the bulk alloy, it was $15 \times 15 \times 15$, and an $11 \times 11 \times 1$ grid of k points was used to calculate low-dimensional structures. Total energy convergence was taken to be achieved if the difference between the total energies of two sequential iterations did not exceed 10^{-5} eV.

The atomic structures of the γ-TiAl(001), (100), and (110) surfaces were modeled by 11-layer thin films separated by 15-Å vacuum region. Low-dimensional structures were optimized by the Newton dynamics to achieve the minimum forces of about 0.01 eV/Å on surface layer atoms. Atomic sites were relaxed both normal to the surface and in planar directions.

The calculations of the total energies of low-dimensional structures were carried out using two models containing two surfaces and one surface. In the model with two surfaces (or the symmetric film model), the atomic sites of three central layers were fixed and the atomic sites of the other layers were optimized to achieve the minimum forces on atoms. In this case, the adsorption energy was calculated by the formula

$$E_{ads} = -\frac{1}{2}[E_{O-TiAl} - E_{TiAl} - E_{O_2}], \qquad (1)$$

where E_{O-TiAl} and E_{TiAl} are the total energies of the systems with and without oxygen, respectively, and E_{O_2} is the total energy of the oxygen molecule. Factor 1/2 demonstrates that oxygen adsorption was considered on both film surfaces. Note that the bond length in the oxygen molecule and the binding energy in it were 1.238 Å and 5.41 eV, which agrees well with the earlier calculation in [32] and the experimental data (1.21 Å, 5.12 eV) in [33].

In the second model, oxygen was considered only on one surface, since three lower atomic layers on the second surface were fixed at the bulk values and the atoms of the other layers could move during structural optimization. In this case, taking into account dipole correction, we were able to compensate for the effects related to film asymmetry. The adsorption energy was estimated as the difference between the total energies of structures with and without oxygen on the surface that was taken with the opposite sign and added to half the total energy of the oxygen molecule.

To estimate the energy barriers for oxygen diffusion in the alloy and from the surface into the bulk of the material, we used the method proposed in [34]. We set initial and final oxygen sites, and intermediate sites were calculated by a linear interpolation. These configurations were called images and were considered to be connected by a spring [35]. All configurations to be calculated were simultaneously relaxed; that is, the optimum site of an oxygen atom and the nearest matrix atoms were determined for each configuration. In this case, the relaxation of each configuration took into account the relaxation of neighboring configurations, which allowed us to find a trajectory with the minimum energy and to determine a saddle point. The diffusion barrier was estimated as the difference between the energies of systems with oxygen in an initial equilibrium state and with oxygen at the saddle point. To study oxygen diffusion in the bulk material, we used the γ-TiAl cell that was doubled along three directions ($2 \times 2 \times 2$) and had 32 atoms and a $9 \times 9 \times 9$ grid of k points. To estimate the oxygen diffusion barriers on a surface and toward the bulk of the material, we used the cell of the same size as in the case of oxygen adsorption in the model with one surface. Test calculations were also performed for the doubled surface supercell.

3. RESULTS AND DISCUSSION

3.1. Oxygen Absorption and Diffusion in γ-TiAl

The intermetallic γ-TiAl alloy has the face-centered $L1_0$ tetragonal structure shown in Fig. 1a. The electronic structure of γ-TiAl was repeatedly studied by the density functional theory [36–40]. Note that the results of present calculations of the structural and electronic properties of the alloy agree well with the results of earlier theoretical and experimental works [36–47]. The calculated lattice parameters of the alloy ($a = 3.989$ Å, $c = 4.068$ Å) agree well with the experimental values ($a = 4.000$ Å, $c = 4.075$ Å) [41]. The enthalpy of alloy formation was determined as the difference between the total energies of the alloy and its components calculated for the hexagonal (Ti) and face-centered cubic (Al) structures. This enthalpy is 0.415 eV/atom and is also in agreement with the calculated value (0.42 eV/atom) obtained in [43] and the experimental value (0.39 ± 0.02 eV/atom) [44].
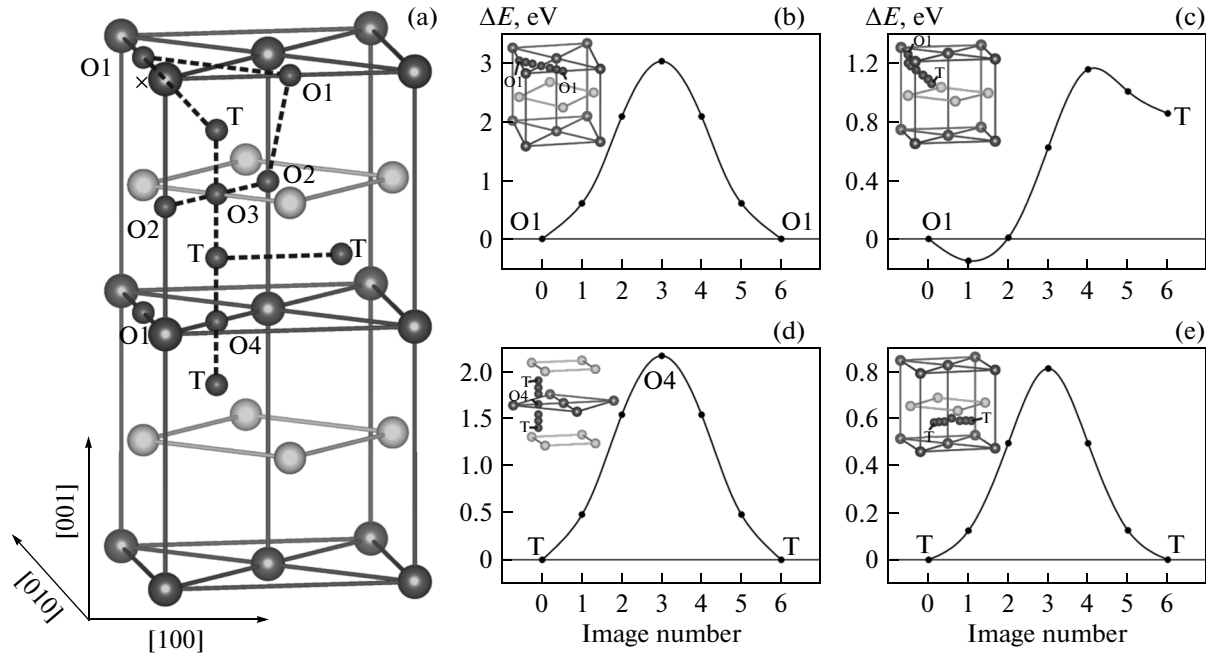
Fig. 1. (a) Atomic structure of the $1 \times 1 \times 2$ cell of a γ-TiAl alloy with octahedral and tetrahedral sites for oxygen and some diffusion profiles in the bulk material: (b) O1 $\longrightarrow$ O1 in the (001) plane, (c) O1 $\longrightarrow$ T, (d) T $\longrightarrow$ T in the [001] direction through saddle point O4, and (e) T $\longrightarrow$ T in the [100] direction. The site corresponding to the minimum in curve (c) is indicated by a cross. The insets to (b)−(d) show the sites of an oxygen atom corresponding to *1−6* along the trajectory with the minimum energy.

Table 1 gives the calculated values of elastic constants C_{ij} and bulk modulus B. To calculate the elastic constants, we used the formalism described in [48] and determined C_{ij} by the formula

$$C_{ij} = \frac{1}{V} \frac{\partial^2 E}{\partial \varepsilon_i \partial \varepsilon_j} \bigg|_{\varepsilon_i, \varepsilon_j = 0}, \quad (2)$$

where E is the total crystal energy, V is the crystal volume, and ε_i is the relative strain. Note that the crystal lattice was sequentially subjected to tetragonal and monoclinic deformation. Bulk modulus B was estimated from the equation

$$B = (C_{11} + 2C_{12})/3. \quad (3)$$

As follows from Table 1, modulus C_{44} agrees well with the experimental data, whereas other elastic constants differ from the experimental values by 8−15%. Elastic constants C_{11}, C_{33}, and C_{66} are lower than the experimental values, and the opposite tendency is found for constants C_{12} and C_{13}. Note that the elastic constants obtained in [45], where the full-potential linearized augmented plane wave method with the local-density approximation for an exchange-correlation potential (FLAPW LDA) was used, are higher than the experimental values except for modulus C_{66}. The energy spectrum and the density of states of the γ-TiAl alloy agree well with the results obtained in [36, 40]; therefore, we do not discuss them here.

The γ-TiAl alloy has the following two types of sites for oxygen sorption: octahedral (O) and tetrahedral (T) sites. There are two types of octahedra: one of which is formed by four titanium atoms and two aluminum atoms, and the other, on the contrary, consists of two titanium atoms and four aluminum atoms. Therefore, we designate the corresponding octahedral sites as O1 and O2, respectively (Fig. 1a). Note that the tetrahedral site (T) has a stoichiometric composition. Calculations showed that site O1 is preferred for oxygen sorption in the bulk material. The absorption energy at this site is 4.02 eV, which is higher that at site O2 by 0.95 eV. The absorption energy was calculated by a formula that was similar to Eq. (1). According to this determination, a higher absorption energy means a stronger bond of oxygen with matrix atoms. The oxygen absorption at site T is higher than at site O2 only by 0.10 eV and is substantially lower than at site O1. Thus, these results demonstrate that oxygen prefers titanium-rich sites in the alloy.

Since the γ-TiAl alloy consists of alternating titanium and aluminum atomic layers in the [001] direction, diffusion paths can be divided into the following two types: along atomic layers in the (001) plane and in the [001] direction (Fig. 1a). Table 2 gives the energy barriers along the paths indicated by dashed lines in Fig. 1a. Some diffusion profiles of oxygen in the bulk material are shown in Figs. 1b−1e. It is seen that the diffusion barrier between the titanium-rich octahedral sites (O1 $\longrightarrow$ O1) in the (001) plane are significantly higher than between the aluminum-rich sites (O2 $\longrightarrow$ O2). Oxygen diffusion is energetically favorable from site O1 to T rather to O2. As is seen in Fig. 1c, the curve near site O1 has a local minimum, which indi-

Table 2. Energy barriers for oxygen diffusion in a γ-TiAl alloy

Diffusion path	Barrier, eV
O1 $\longrightarrow$ O1	3.02
O2 $\longrightarrow$ O2	0.10
O1 $\longrightarrow$ O2	1.64
O1 $\longrightarrow$ T	1.15
T $\longrightarrow$ O1	0.30
T $\longrightarrow$ O2	0.19
T $\longrightarrow$ O3 $\longrightarrow$ T	0.08
T $\longrightarrow$ O4 $\longrightarrow$ T	2.17
T $\longrightarrow$ T	0.81

cates that the oxygen site indicated by the cross in Fig. 1a is more stable than O1. The difference between the energies of oxygen sorption at this site and O1 is only 0.15 eV. It should be noted that diffusion in the opposite direction is easier due to the asymmetric diffusion profile O1 $\longrightarrow$ T (Fig. 1c). During oxygen diffusion through tetrahedral interstices along the [001] direction, a saddle point can be located between aluminum (O3) or titanium (O4) atoms. As follows from Table 2, the energy barrier is substantially lower during diffusion through an aluminum layer than through a titanium layer, which can be a trap for oxygen. We also considered a path between tetrahedral interstices along the [100] direction between a titanium and an aluminum layer. In this case, the energy barrier is 0.81 eV, which is substantially lower than the barrier through the titanium layer (2.17 eV). On the whole, an analysis of these results allows us to conclude that the optimum diffusion path of oxygen in the [001] direction passes along tetrahedral interstices through the aluminum layer and through an octahedral interstice

Fig. 2. Surface energy of a low-index surface in a γ-TiAl alloy vs. the chemical potential of aluminum.

(T $\longrightarrow$ O1 $\longrightarrow$ T) in the titanium layer. In the (001) plane, oxygen can diffuse along octahedral interstices in the aluminum layer and along tetrahedral interstices.

3.2. Energy Stability of Low-Index TiAl Surfaces

It is seen in Fig. 1a that the TiAl(001) surface can be terminated by a titanium (TiAl(001)$_{Ti}$) or an aluminum (TiAl(001)$_{Al}$) layer. We will use similar designations for the TiAl(110) surface. Each atomic layer along the [100] direction contains both alloy components. Figure 2 shows surface energy σ as a function of the chemical potential of Al for the low-index surfaces under study. Recall that the surface energy is calculated by the formula

$$\sigma = \frac{1}{2S}(E_{\text{tot}}^{\text{slab}} - NE_{\text{tot}}^{\text{bulk}}), \qquad (4)$$

where $E_{\text{tot}}^{\text{bulk}}$ is the total alloy energy, $E_{\text{tot}}^{\text{slab}}$ is the energy of the cell containing a thin film and vacuum, and S is the surface area. Note that Eq. (4) is valid only for stoichiometric surfaces. In the case of nonstoichiometric surfaces, σ is calculated as follows:

$$\sigma = \frac{1}{2S}[E_{\text{tot}}^{\text{slab}} - N_{\text{Ti}}\mu_{\text{Ti}} - N_{\text{Ti}}\mu_{\text{Al}}], \qquad (5)$$

where N_{Ti} and N_{Al} are the numbers of Ti and Al atoms, respectively, and μ_{Ti} and μ_{Al} are the chemical potentials of Ti and Al, respectively. In turn, Eq. (5) can be rewritten as a function of one variable, e.g., the chemical potential of aluminum,

$$\sigma = \frac{1}{2S}[E_{\text{tot}}^{\text{slab}} - N_{\text{Ti}}\mu_{\text{TiAl}} - \mu_{\text{Al}}(N_{\text{Al}} - N_{\text{Ti}})], \qquad (6)$$

where $\mu_{\text{TiAl}} = \mu_{\text{Ti}} + \mu_{\text{Al}}$. It is known that the chemical potentials of the alloy components are lower than the chemical potentials of the corresponding pure elements in the crystalline state, $\Delta\mu_{\text{Al}} = \mu_{\text{Al}} - \mu_{\text{Al}}^{\text{bulk}} \leq 0$. It should be noted that $\Delta\mu_{\text{Al}}$ changes in the range $-\Delta H \leq \Delta\mu_{\text{Al}} \leq 0$, where ΔH (0.829 eV) is the enthalpy of TiAl formation. Equation (6) can be rewritten as a function of $\Delta\mu_{\text{Al}}$,

$$\sigma = \frac{1}{2S}[E_{\text{tot}}^{\text{slab}} - N_{\text{Ti}}\mu_{\text{TiAl}} - \mu_{\text{Al}}^{\text{bulk}}(N_{\text{Al}} - N_{\text{Ti}}) \\ - \Delta\mu_{\text{Al}}(N_{\text{Al}} - N_{\text{Ti}})]. \qquad (7)$$

To determine the chemical potentials of the alloy components, we used a face-centered cubic structure for aluminum and a hexagonal structure for titanium.

As is seen in Fig. 2, the TiAl(100) surface is most stable in a titanium-rich region, and the TiAl(110) surface termination by aluminum is stable in an aluminum-rich region. In the limit of high aluminum concentrations, the surface energies of TiAl(001)$_{Al}$ and TiAl(110)$_{Al}$ are almost the same. It should be noted that, in contrast to the (110) surface, the TiAl(011) surface is stoichiometric. However, its energy is higher
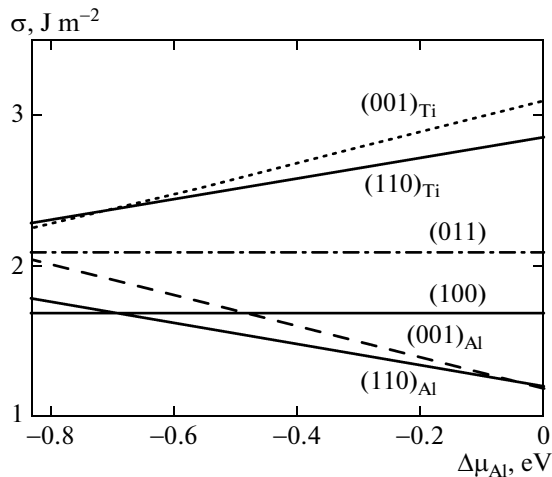
than that of (100), and we will not consider it from here on. When testing the surface energy convergence as a function of the number of atomic layers (from 7 to 15), we found that σ converges rapidly when the number of atomic layers increases and that 11-layer films well describe the structures under study. The surface energies agree well with the projector augmented wave (PAW-GGA) calculation [49]. In particular, the surface energy of TiAl(100) (1.70 J/m²) agrees well with the value (1.62 J/m²) obtained in [49], whereas a higher value (1.91 J/m² [39]) was obtained in the calculation with the local-density approximation for an exchange-correlation functional (PAW-LDA).

Fig. 3. Oxygen adsorption sites indicated by crosses on nonstoichiometric (001) and (110) surfaces and on stoichiometric (100) surface. Symbols H, B, and T indicate hollow, bridge, and top sites, respectively, on the surfaces. Light and dark balls correspond to aluminum and titanium atoms, respectively.

3.3. Oxygen Adsorption on the (001), (100), and (110) TiAl Surfaces

Figure 3 shows the considered high-symmetry sites for oxygen adsorption on some TiAl surfaces. We analyzed hollow (H), bridge (B), and top (T) sites, which have the same coordination on various surfaces. As follows from Table 3, oxygen adsorption on the TiAl(001)$_{Ti}$ surface is preferred at a hollow H site, whereas the bridge B site between two aluminum atoms is preferred on the TiAl(001)$_{Al}$ surface. The difference between the energies of oxygen adsorption at sites B and H in TiAl(001)$_{Al}$ is only 0.2 eV. A higher binding energy of oxygen on the TiAl(001)$_{Ti}$ surface as compared to the binding energy on the TiAl(001)$_{Al}$ surface indicates that, as in the bulk alloy, oxygen on the surface prefers titanium-rich sites (Table 3). This conclusion agrees with the experimental data in [50], which showed that oxygen adsorbs near aluminum sites only when the oxygen concentration increases. On the stoichiometric TiAl(100) surface, oxygen adsorption at site H$_{Al}$ over a subsurface aluminum atom is only slightly preferable as compared to the site over a subsurface titanium atom (H$_{Ti}$). It is interesting that the maximum hydrogen adsorption energy was also obtained at site H$_{Al}$ [39]. Oxygen shifts to hollow site H$_{Al}$ on the (100) surface during relaxation from the bridge site between titanium and aluminum atoms. Oxygen adsorption at long bridge site B1 is preferred for the (110) surface irrespective of its termination. As follows from Table 3, oxygen adsorption is less prefer-
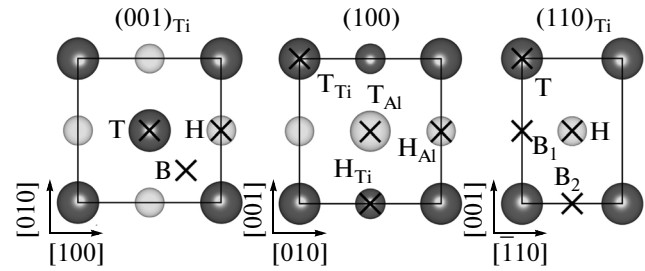
able at top sites. On the whole, the results obtained in terms of the two calculation models agree well with each other in the adsorption energy, the relaxation of interplanar spacings, and the position of oxygen relative to a surface.

3.4. Electronic and Structural Factors

The preference of certain sites for oxygen adsorption on low-index alloy surfaces can be explained when analyzing electron and structural characteristics. We now briefly discuss the electron characteristics obtained for the stoichiometric γ-TiAl(100) surface as an example. Figure 4 shows local densities of states (DOS) for oxygen and the alloy components at the studied sorption sites on the (100) surface. Note that the adsorption of one oxygen atom on the (100) surface corresponds to a coverage of 0.5 monolayer (ML).

As is seen in Fig. 4, oxygen predominantly interacts with the metallic atoms of the surface layer. This interaction leads to the appearance of peaks in the local DOS of Ti and Al surface atoms, the energy positions of which coincide with those of the corresponding peaks of the s and p states of oxygen. The valence band of oxygen is known to consist of two subbands. The sharp peak caused by the s states of oxygen is located at energies from −21 to −16 eV depending on the site of oxygen sorption. The center of gravity of the p band of

Table 3. Oxygen adsorption energies (eV) on the γ-TiAl(001), (100), and (110) surfaces. The values of E_{ads} calculated using the symmetric film model are given in parentheses

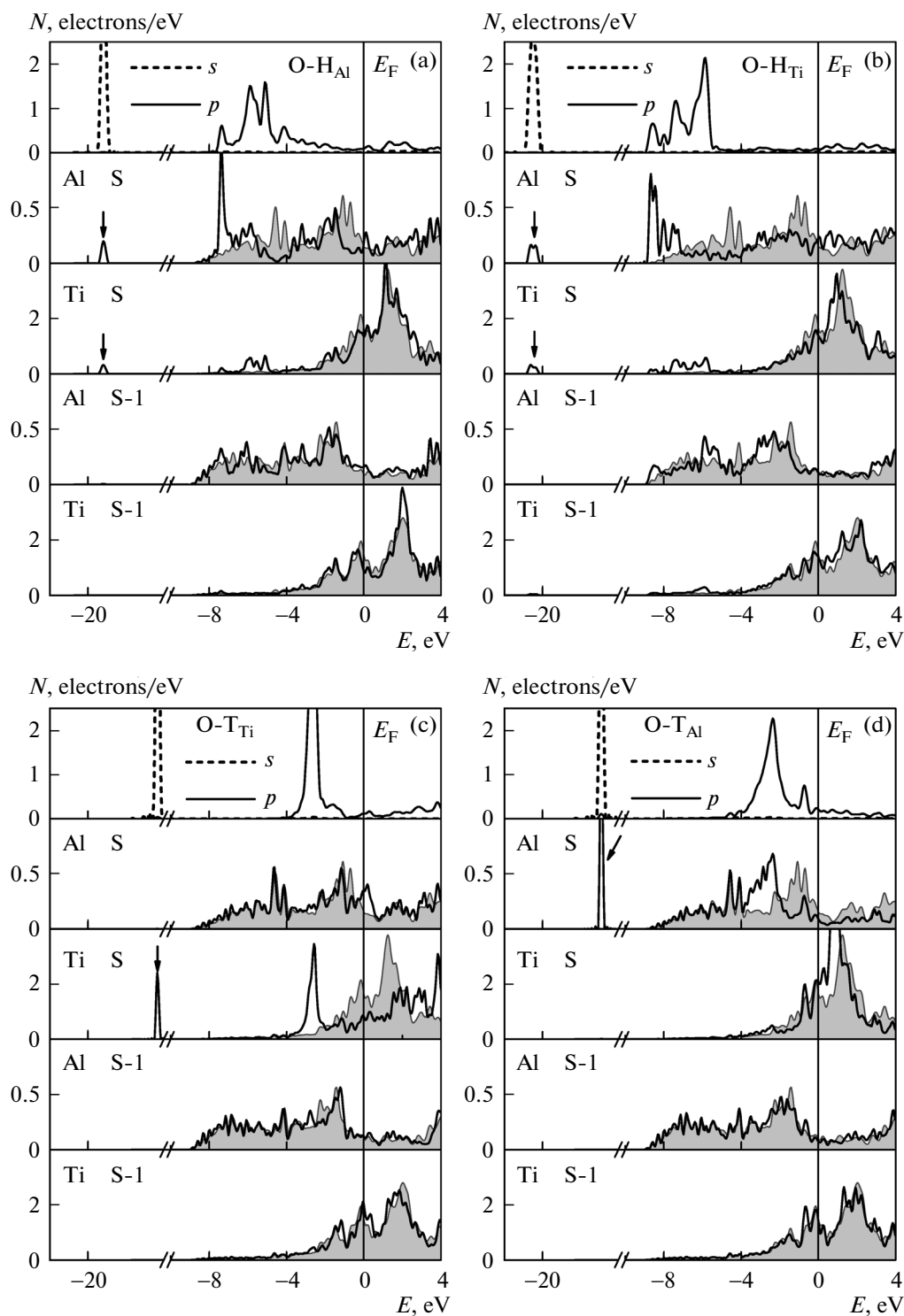| Site	H	B (B1)	B2	T
TiAl(001)$_{Ti}$	6.157 (6.147)	5.481 (5.479)	−	4.139 (4.119)
TiAl(001)$_{Al}$	4.020 (4.012)	4.211 (4.212)	−	2.138 (2.099)
TiAl(110)$_{Ti}$	4.811	5.945	4.587	4.348
TiAl(110)$_{Al}$	2.660	4.673	4.352	1.501
Site	H$_{Al}$	H$_{Ti}$	T$_{Ti}$	T$_{Al}$
TiAl(100)	4.851 (4.859)	4.632 (4.633)	3.430 (3.393)	2.510 (2.503)

Fig. 4. Local DOS of oxygen and metals in the surface (S) and subsurface (S-1) layers vs. the site of oxygen adsorption on the TiAl(100) surface. Local DOSs of Ti and Al in the case of the pure surface are gray.

oxygen is seen to shift toward the Fermi level during oxygen sorption at top sites as compared to more preferable hollow sites. The strong hybridization of the s and p states of oxygen with the orbitals of both metals causes the preference of hollow sites for oxygen

adsorption. On the whole, the changes of an electronic structure for two hollow sites are similar. The following processes take place: the appearance of small peaks caused by an interaction with the s orbitals of oxygen (indicated by arrows in Fig. 4), low metallic states are

split due to their interaction with the p orbitals of oxygen, and a pseudogap forms. These processes are most pronounced in the case of adsorption at hollow sites. It is seen in Fig. 4a that a pseudogap forms at an energy of -4.5 eV during oxygen adsorption at H_{Al} sites. The splitting off of titanium states from the valence band bottom of a metal is most pronounced for oxygen adsorption at the H_{Ti} site (Fig. 4b). The split states are in the energy range from -8.8 to -5.6 eV. The hybridization between the orbitals of the metals and oxygen at top sites is less pronounced; moreover, the p_z orbitals of Al and the d_{z^2} orbitals of Ti, which provide an interaction with oxygen at these sites, are almost unoccupied (Figs. 4c, 4d). Therefore, the interaction of oxygen with the surface at these sites is less favorable, which is reflected by the adsorption energies.

The interaction with the atoms of the subsurface layer is indirect, through hybridization with the orbitals of surface atoms. It is seen that the local DOS of subsurface atoms change more weakly than those of surface atoms as compared to the DOS of the pure surfaces. The DOS of a subsurface aluminum atom during oxygen adsorption at site H_{Ti} changes most strongly, which is related to the causes noted above, namely, hybridization with the states of a surface titanium atom. The appearance of the titanium states in the range from -8.8 to -5.6 eV that are induced by an interaction with the p orbitals of oxygen leads to the appearance of new hybridized states of aluminum from the subsurface layer in this energy range, which causes a shift of its states from the Fermi level.

When calculating partial DOS, we can determine the symmetry of the states involved in an interaction with oxygen, since they change most substantially as compared to the states of the pure surface. An example of such an analysis was given in our work [51]. The calculations performed in this work also showed that a charge $\sim 1.5e$ is transferred from the surface to oxygen at hollow sites and a charge of only $0.7e$ is transferred at the top site above titanium. The preference of site H_{Al} is likely to be mainly caused by structural factors, namely, a large distance between titanium atoms in the [001] direction. At this site oxygen is located at a distance of 0.25 Å from the surface, and it is located significantly higher (at a distance of 0.66 Å from the surface) at site H_{Ti}.

The interaction of oxygen with an alloy surface results in partial removal of the negative relaxation of the interlayer distances detected on pure surfaces. The compression of the first interplanar spacing from -2.46 to -2.56% (-2.16% [39]) was obtained for the Ti and Al sublattices, respectively, in the case of a pure surface. As a result of oxygen adsorption at hollow sites H_{Ti} and H_{Al}, the interplanar spacing is restored to almost the bulk spacing (-0.03 and $+0.07\%$, respec-

tively). The aluminum atoms on the pure γ-TiAl(100) surface shift by approximately 0.05 Å relative to titanium atoms, and the splitting of the surface layer increases to 0.17 Å at site H_{Al}.

We now consider the change in the atomic and electron structures of γ-TiAl(100) when the oxygen concentration increases to 2 ML. In this case, we can use the following two approaches: to sequentially analyze the adsorption of molecular oxygen on the surface, as was done in [22–24] (where the initial stage of oxidation of the TiNi(110) surface was studied), or to use the approach proposed in [25] for the TiAl(111) surface. The authors of [25] investigated the filling of the most preferred sites on the surface and in the surface layers with oxygen atoms. Obviously, the first approach is more consistent but it requires a longer computer time. Therefore, we chose the second approach to gain an impression of how the oxygen concentration affects the electronic characteristics of TiAl(100). In this case, the second oxygen atom was placed at the second (in energy preference) H_{Ti} site.

Figure 5 shows the atomic structures and the DOS of Al and Ti surface atoms as a function of the oxygen concentration. It is seen in Fig. 5b that, as the oxygen concentration increases to 1 ML, an oxidelike layer forms on the surface. The adsorption energy of the second oxygen atom increases insignificantly (4.931 eV/atom) as compared to E_{ads} of the first oxygen atom. The adsorption of the second atom leads to substantial changes in the local DOS of titanium and aluminum surface atoms (Figs. 5c, 5d). First of all, we now analyze the changes of the DOS of titanium atoms induced by an increase in the oxygen concentration on the surface. It is seen in Fig. 5c that the electronic states near the Fermi level are split to form a pseudogap in the range from -5 to -2.5 eV. This effect is also observed for the lower states near -19 eV. Actually, a certain peak of these states can be attributed to each oxygen atom on the surface. Since a further increase in the oxygen concentration favors its penetration into the subsurface layers (which was supported by our preliminary calculations of the sorption of molecular oxygen), we calculated the total energies of several configurations with oxygen in the subsurface layers. These configurations differed in the sites of oxygen atoms on the surface and in the region between the surface and subsurface layers. This analysis allowed us to determine the most preferred configurations (Figs. 5e, 5f). As a result of the filling of subsurface sites with oxygen, the number of the lower states that reflect the interaction of the s orbitals of oxygen with the s and d states of surface Ti increases substantially, and the gap characteristic of metallic oxides continues to form. The splitting off of states from the valence band bottom of the metal below -2.5 eV is mainly caused by an interaction with the p orbitals of oxygen and means the formation of new Ti–O bonds and a weakening of the metallic Ti–Al bonds on the alloy surface. The introduction of oxygen into the subsur-
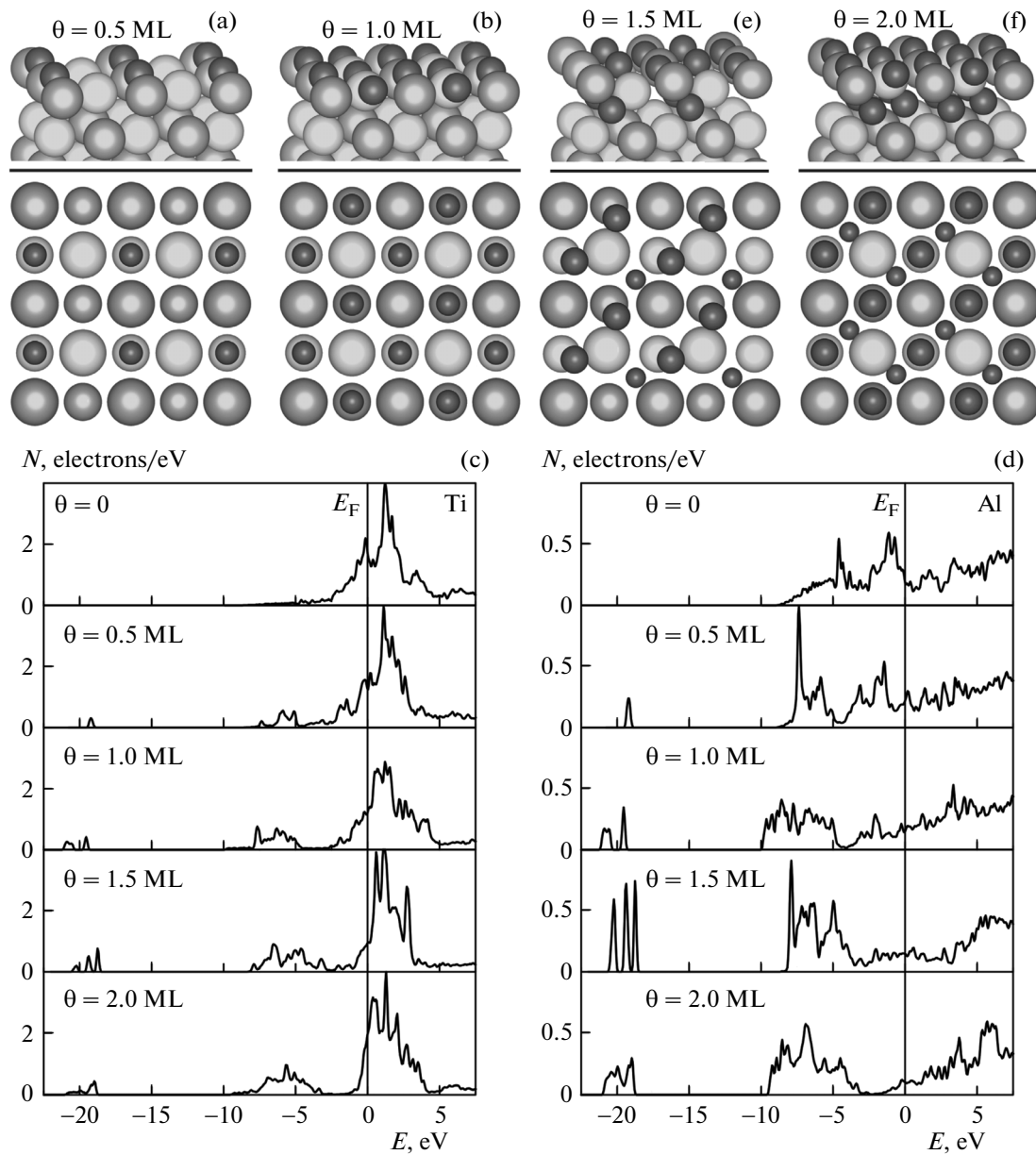
Fig. 5. Atomic structure of the TiAl(100) surface with oxygen (a), (b), (e), (f) from 0.5 to 2 ML and the change of the local DOS of (c) Ti and (d) Al induced by an increase in the oxygen concentration.

face layers is known to point to the initial stage of surface oxidation. Note that the binding energy of a subsurface oxygen atom is lower than that of surface atoms by 0.25 eV/atom for a coverage of 1.5 ML. The electrostatic interaction leads to the shift of oxygen atoms on the surface from hollow sites for a given oxygen concentration (Fig. 5e). In this case, aluminum atoms are threefold coordinated by oxygen atoms, as in Al_2O_3, and the Al−O bond length (1.82 Å) is almost identical to that in aluminum oxide. As is seen in Fig. 5c, the states of titanium at a given oxygen coverage shift toward high energies and are almost unoccupied. As the oxygen concentration increases, the

pseudogap also shifts toward the Fermi level and forms completely for a coating of 2 ML, where two of the four atoms are located between the surface and the subsurface layers (Fig. 5f). It is seen, however, that Ti states are retained at the Fermi level, which indicates a metallic character of the surface. Similar behavior is observed for the Al states; however, O−Ti bonds form easier than O−Al bonds, which is indicated by the fact that a pseudogap forms in the titanium states even for monolayer coverage (Fig. 5d). Since states in the gap are almost absent for the TiAl(111) surface at two oxygen monolayers [25], we can conclude that the forma-
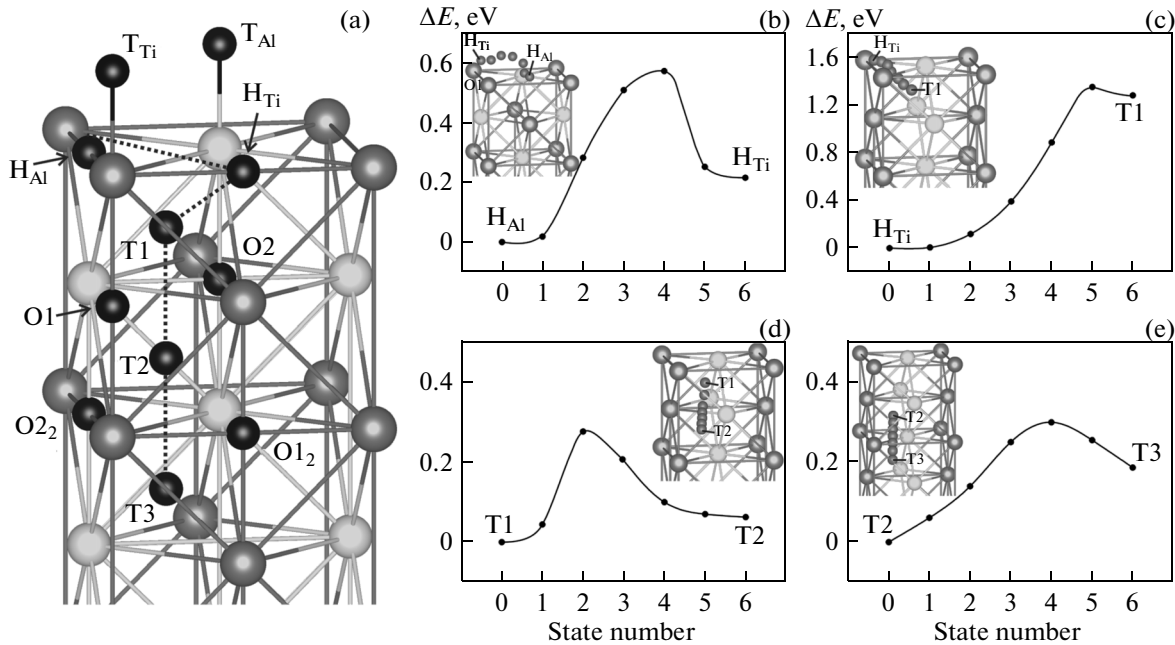
Fig. 6. (a) Schematic representation of the oxygen sites on the TiAl(100) surface and in the subsurface layers and (b)−(e) diffusion profiles along certain directions. Ti, Al, and O atoms are represented by gray, light gray, and black balls, respectively.

tion of oxide layers on the (100) surface is more complex.

3.5. Oxygen Diffusion on the TiAl(100) Surface

We now discuss oxygen diffusion paths on the TiAl(100) surface and deep into the alloy. Figure 6a shows the sites of an oxygen atom under study. Note that the sites in the surface layer are given schematically, since an oxygen atom at equilibrium sites is located at certain distances (0.25−1.65 Å) from the surface layer. Moreover, we only show part of the supercell used to calculate the alloy surface. An energy barrier of 0.57 eV was calculated for oxygen diffusion along the $H_{Al} \longrightarrow H_{Ti}$ direction in the surface layer. Note that this value is higher than the hydrogen diffusion barrier on the surface by 0.25 eV [39]. At the same time, the energy barrier to oxygen diffusion in the surface layer is significantly lower than the diffusion barrier to the subsurface layer (Table 4).

It follows from Table 4 that the barriers to oxygen diffusion from the tetrahedral (T1) to the octahedral (O1, O2) sites are low and differ insignificantly from each other. However, the diffusion between the tetrahedral sites (T1 $\longrightarrow$ T2) is energetically preferable as compared to the diffusion to the octahedral sites of the subsurface layer. The oxygen diffusion between the octahedral sites of the subsurface layer and the layer next to the surface is less favorable than that on the surface, and the barrier increases with the distance from the surface. The barriers also increase if an initial oxygen site was located in a titanium-rich region,

which indicates the preference of Ti−O bond formation and agrees with the experimental data in [50]. In particular, the barrier between sites O1 and T2 is 1.15 eV, and the O2 $\longrightarrow$ T2 barrier is lower by an order of magnitude. An analysis of these results allows us to conclude that the optimum diffusion path of an oxygen atom from the γ-TiAl(100) surface to the material volume is $H_{Al} \longrightarrow H_{Ti} \longrightarrow T1 \longrightarrow T2 \longrightarrow T3$. This conclusion differs from the conclusion drawn earlier for hydrogen diffusion in [39], since the diffusion between tetrahedral sites was not considered in that work.

In conclusion, we note that an increase in the supercell size is not reflected on the detected tenden-

Table 4. Energy barriers for oxygen diffusion on the TiAl(100) surface and in the subsurface layers

Diffusion path	Barrier, eV	Diffusion path	Barrier, eV
$H_{Al} \longrightarrow H_{Ti}$	0.57	$T1 \longrightarrow T2$	0.28
$H_{Al} \longrightarrow T1$	1.63	$T2 \longrightarrow O2_2$	0.27
$H_{Ti} \longrightarrow T1$	1.35	$T2 \longrightarrow O1_2$	0.11
$T1 \longrightarrow O1$	0.32	$O2_2 \longrightarrow O1_2$	1.02
$T1 \longrightarrow O2$	0.31		
$O1 \longrightarrow O2$	0.97	$O2_2 \longrightarrow T3$	0.12
		$O1_2 \longrightarrow T3$	1.13
$O1 \longrightarrow T2$	1.15	$T2 \longrightarrow T3$	0.30
$O2 \longrightarrow T2$	0.09		

cies and changes the energy barriers by 5−10%. In particular, the energy barrier between the sites in the surface layer increases from 0.57 to 0.62 eV and the minimum barrier (O2 $\longrightarrow$ T2) decreases from 0.09 to 0.08 eV.

4. CONCLUSIONS

We presented the results of the calculation of oxygen sorption in a γ-TiAl alloy on low-index (001), (100), and (110) surfaces that was performed by the pseudopotential method in a plane-wave basis. The oxygen sorption in a γ-TiAl alloy was shown to be preferred in a titanium-rich octahedral site. Oxygen prefers to adsorb at bridge site B on the TiAl(001)$_{Al}$ surface, which is stable in the limit of high aluminum concentrations, an hollow site H is preferred for oxygen on TiAl(001)$_{Ti}$. On the stoichiometric TiAl(100) surface, the adsorption energy is also maximal for the hollow site above a subsurface aluminum atom. Oxygen prefers to adsorb at long bridge site B1 on the TiAl(110) surface irrespective of its termination. Using the stoichiometric (100) surface as an example, we discussed the changes of the structural and electronic characteristics induced by oxygen adsorption, including the changes caused by an increase in the oxygen concentration. It was shown that one oxygen monolayer on the (100) surface is insufficient for its saturation. An increase in the oxygen concentration leads to the penetration of oxygen into the subsurface layers, where it occupies tetrahedral sites. The binding energy of subsurface oxygen atoms is lower than on the surface. The appearance of new Ti−O and Al−O bonds is accompanied by the formation of a bandgap and a weakening of the Ti−Al metallic bonds in the alloy. Calculations demonstrate that the formation of Ti−O bonds prevails over aluminum oxidation when the oxygen concentration increases. On the whole, mixed oxide layers can form on the (100) surface, which agrees with the experimental data in [6, 7, 13]. The calculations of the diffusion paths from the (100) surface to the material volume showed that diffusion on the surface is preferred as compared to diffusion into the subsurface layers. After the penetration of oxygen into the subsurface layer, oxygen migration along tetrahedral interstices is preferred. The energy barriers increase for diffusion from titanium-rich sites.

Obviously, the processes that occur on the γ-TiAl alloy surface are complex and should be considered on various scale levels. In this work, we only considered the microscopic aspect of the interaction of oxygen on the low-index surfaces and energy in the bulk of the γ-TiAl alloy and did not take into account many effects, including the effect of temperature and the structural transformations on the surfaces. Nevertheless, ab initio calculations allowed us to correctly estimate the oxygen sorption energy in the bulk and on the surface and to predict the microscopic mechanism of gas diffusion, information on which can hardly be obtained from experimental data. In further studies, we are going to take into account the effect of structural defects and alloying metals and to consider the oxidation of the alloy surface in more detail.

REFERENCES

1. A. Takasaki, Y. Furuya, and Y. Taneda, Mater. Sci. Eng., A **239−240**, 265 (1997).

2. K. Hashi, K. Ishikawa, K. Suzuki, and K. Aoki, J. Alloy Comp. **330−332**, 547 (2002).

3. F. H. Froes, C. Suryanarayana, and D. Eliezer, J. Mater. Sci. **27**, 5113 (1992).

4. F. Appel and R. Wagner, Mater. Sci. Eng., R **22**, 187 (1998).

5. F. Appel, J. D. Heaton-Paul, and M. Oehring, *Gamma Titanium Aluminide Alloys* (Wiley, Singapore, 2011), p. 762.

6. S. Becker, A. Rahmel, W. J. Quadakkers, M. Schorr and M. Schütze, Oxid. Met. **38**, 425 (1992).

7. M. Schmitz-Niederau and M. Schütze, Oxid. Met. **52**, 225 (1999).

8. C. Lang and M. Schütze, Oxid. Met. **46**, 255 (1996).

9. C. Lang and M. Schütze, Mater. Corros. **48**, 13 (1997).

10. J. P. Lin, L. L. Zhao, G. Y. Li, L. Q. Zhang, X. P. Song, F. Ye, and G. L. Chen, Intermetallics **19**, 131 (2011).

11. P. K. Datta, H. L. Du, J. S. Burnell-Gray, and R. E. Ricker, *ASM Handbook*, Vol. 13B: *Corrosion Materials* (ASM International, Materials Park, Ohio, United States, 2005), p. 490.

12. M. Goral, L. Swadzba, G. Moskal, G. Jarczyk, and J. Aguilar, Intermetallics **19**, 744 (2011).

13. K. Przybylski, J. Prażuch, T. Brylewski, et al., Arch. Metall. Mater. **2**, 477 (2013).

14. A. Kiejna and B. I. Lundqvist, Phys. Rev. B: Condens. Matter **63**, 085405 (2001).

15. A. Kiejna and B. I. Lundqvist, Surf. Sci. **504**, 1 (2002).

16. M. V. Ganduglia-Pirovano and M. Scheffler, Phys. Rev. B: Condens. Matter **59**, 15533 (1999).

17. K. Reuter, M. V. Ganduglia-Pirovano, C. Stampfl, and M. Scheffler, Phys. Rev. B: Condens. Matter **65**, 165403 (2002).

18. W. X. Li, C. Stampf, and M. Scheffler, Phys. Rev. B: Condens. Matter **65**, 075407 (2002).

19. V. Blum, L. Hammer, C. Schmidt, W. Meier, O. Wieckhorst, S. Müller, and K. Heinz, Phys. Rev. Lett. **89**, 266102 (2002).

20. A. Y. Lozovoi, A. Alavi, and M. W. Finnis, Phys. Rev. Lett. **85**, 610 (2000).

21. S. E. Kulkova, V. E. Egorushkin, S. V. Eremeev, and S. S. Kulkov, Mater. Sci. Eng., A **438**, 476 (2006).

22. M. Nolan and S. A. M. Tofail, Biomaterials **31**, 3439 (2010).

23. M. Nolan and S. A. M. Tofail, Phys. Chem. Chem. Phys. **12**, 9742 (2010).

24. S. E. Kulkova, A. V. Bakulin, Q. M. Hu, and R. Yang, Physica B (Amsterdam) **426**, 118 (2013).

25. H. Li, S. Wang, and H. Ye, J. Mater. Sci. Technol. **25**, 569 (2009).

26. S. Y. Liu, J. X. Shang, F. H. Wang, and Y. Zhang, Phys. Rev. B: Condens. Matter **79**, 075419 (2009).

27. G. Kresse and J. Hafner, Phys. Rev. B: Condens. Matter **48**, 13115 (1993).

28. G. Kresse and J. Furthmüller, Phys. Rev. B: Condens. Matter **54**, 11169 (1996).

29. G. Kresse and J. Furthmüller, Comput. Mater. Sci. **6**, 15 (1996).

30. J. P. Perdew, J. A. Chevary, S. H. Vosko, K. A. Jackson, M. R. Pederson, D. J. Singh, and C. Fiolhais, Phys. Rev. B: Condens. Matter **46**, 6671 (1992).

31. H. J. Monkhorst, J. A. Chevary, S. H. Vosko, et al., Phys. Rev. B: Solid State **13**, 5188 (1976).

32. H. Shi and C. Stampfl, Phys. Rev. B: Condens. Matter **76**, 075327 (2007).

33. K. P. Huber and G. Herzberg, *Molecular Spectra and Molecular Structure: IV. Constants of Diatomic Molecules* (Van Nostrand Reinhold, New York, 1979).

34. G. Mills, H. Jonsson, and G. K. Schenter, Surf. Sci. **324**, 305 (1995).

35. G. Henkelman, B. P. Uberuaga, and H. Jónsson, J. Chem. Phys. **113**, 9901 (2000).

36. S. D. Chebb, D. A. Papaconstantopolus, and B. M. Klein, Phys. Rev. B: Condens. Matter **38**, 12120 (1988).

37. R. R. Zope and Y. Mishin, Phys. Rev. B: Condens. Matter **68**, 024102 (2003).

38. E. A. Smirnova, E. I. Isaev, and Yu. Kh. Vekilov, Phys. Solid State **46** (8), 1383 (2004).

39. J. W. Wang and H. R. Gong, Int. J. Hydrogen Energy **39**, 6068 (2014).

40. A. Hussain, S. S. Hayat, and M. A. Choudhry, Physica B (Amsterdam) **406**, 1961 (2011).

41. J. Braun and M. Ellner, Metall. Mater. Trans. A **32**, 1037 (2001).

42. T. Sikora, G. Hug, M. Jaouen, and J. J. Rehr, Phys. Rev. B: Condens. Matter **62**, 1726 (2000).

43. J. Zou, C. L. Fu, and M. H. Yoo, Intermetallics **3**, 265 (1995).

44. R. Hultgren, P. D. Desai, D. T. Hawkins, M. Gleiser, and K. K. Kelley, *Selected Values of the Thermodynamic Properties of Binary Alloys* (American Society for Metals, Materials Park, Ohio, United States, 1973).

45. C. L. Fu and M. H. Yoo, Philos. Mag. Lett. **62**, 159 (1990).

46. K. Tanaka, Philos. Mag. Lett. **73**, 71 (1996).

47. Y. He, R. B. Schwarz, T. Darling, M. Hundely, S. H. Whang, and S. C. Wang, Mater. Sci. Eng., A **239–240**, 157 (1997).

48. Y. L. Page and P. Saxe, Phys. Rev. B: Condens. Matter **65**, 104104 (2002).

49. L. Wang, J. X. Shang, F. H. Wang, Y. Zhang, and A. Chroneos, J. Phys.: Condens. Matter. **23**, 265009 (2011).

50. M. R. Shanabarger, Appl. Surf. Sci. **134**, 179 (1998).

51. S. S. Kulkov, A. V. Bakulin, and S. E. Kulkova, J. Exp. Theor. Phys. **119** (3), 521 (2014).

Translated by K. Shakhlevich